Li ion diffusion mechanisms in the crystalline electrolyte γ-Li_3PO_4

Yaojun A. Du* and N. A. W. Holzwarth†

Department of Physics, Wake Forest University,

Winston-Salem, North Carolina 27109, USA

(Dated: June 20, 2007)

Abstract

Solid state lithium ion electrolytes are becoming increasingly important in batteries and related technologies. We have used first-principles modeling techniques based on density functional theory and the nudged elastic band method to examine possible Li ion diffusion mechanisms in idealized crystals of the electrolyte material Li_3PO_4. In modeling the Li ion vacancy diffusion, we find direct hopping between neighboring meta-stable vacancy configurations to have a minimal migration barrier of $E_m = 0.6$ eV. In modeling the Li ion interstitial diffusion, we find an interstitialcy mechanism, involving the concerted motion of an interstitial Li ion and a neighboring Li ion of the host lattice, that can result in a migration barrier as low as $E_m = 0.2$ eV. The minimal formation energy of a Li ion vacancy-interstitial pair is determined to be $E_f = 1.6$ eV. Assuming the activation energy for intrinsic defects to be given by $E_A = E_m + E_f/2$, the calculations find $E_A = 1.0 - 1.2$ eV for ionic diffusion in crystalline γ-Li_3PO_4, in good agreement with reported experimental values of 1.1-1.3 eV.

PACS numbers: 82.45.Gj, 82.47.Aa, 71.15.Pd, 71.15.Nc, 66.10.Ed, 66.30.-h, 66.30.Dn, 66.30.Hs, 66.30.Jt, 66.30.Lw

Keywords: electrolyte, lithium battery, nudged elastic band method, density functional calculation

*duy@wfu.edu

†natalie@wfu.edu

I. INTRODUCTION

Recently, there has been a lot of interest in solid electrolyte materials which are permeable to Li ions (Li^+) and impermeable to electrons for use in batteries and related technologies. In particular, the LiPON electrolyte material based on Li_3PO_4 was developed at Oak Ridge National Laboratory.[1–4] Because of its chemical and physical stability, it can be reliably used in very thin films in a variety of applications.[5]

In order to better understand the properties of these materials, we have used first-principles modeling techniques to examine possible Li ion diffusion mechanisms in idealized crystals of Li_3PO_4. We report on our study of several plausible diffusion processes, considering vacancy and interstitial ion motions. The outline of the paper is as follows. Section II describes the crystal structure examined in the present work and details the computational methods. Results are presented in Sec. III, with separate discussions of vacancy motion (III A), interstitial motion (III B), and formation energies for vacancy-interstitial defect pairs (III C). Conclusions are presented in Sec. IV, where the calculation results for the ideal crystals models are related to the experimental literature and electrolyte properties.

II. CALCULATIONAL METHODS

There are two well-characterized crystalline forms of Li_3PO_4 which are labeled β and γ.[3, 6–8] An α form is mentioned in the literature,[9] but its crystal structure has not been completely determined. This study focuses on the γ form, which is thermodynamically less stable than the β form,[10] but which is sufficiently metastable to be observed and measured at room temperature by several experimental groups.

Crystalline γ-Li_3PO_4 has the orthorhombic Pnma structure (62).[11] Figure 1 shows a

ball and stick drawing of 4 unit cells of the ideal crystal. The Li ions are located on two crystallographically different sites indicated with different shadings in the figure. Using the Wyckoff labels, the d site accounts for 8 equivalent Li ions and the c site accounts for 4 equivalent Li ions per unit cell. Table I lists the lattice parameters and the fractional coordinates of the inequivalent atoms for this structure.

The energy calculations performed in this study are based on density functional theory[12, 13] and are carried out using the Quantum ESPRESSO (*PWscf*) package[14] and the ultrasoft pseudopotential formalism of Vanderbilt.[15] The pseudopotentials for Li, P, and O are constructed using the USPP code[15] and tested for agreement with calculations using other methods and codes.[16, 17] The form of the exchange-correlation functional is taken to be the generalized gradient (GGA) form.[18, 19] Visualizations of the structures are obtained using XCrySDen[20] and OpenDX[21] software.

For the perfect crystal, the lattice constants calculated using variable cell optimization[22] are given in Table I and compared with experimental values. The calculated values are approximately 1% larger than experiment as is consistent with our experience using the GGA to study similar materials (while the local density approximation (LDA) generally underestimates the lattice constants).[17] The calculated internal coordinates of the inequivalent sites are found to agree with the experimental values of the fractional coordinates within ± 0.004.

The results reported here are obtained using the supercell shown in Fig. 1 having dimension $a \times 2b \times 2c$. The planewave expansions are truncated with wavevectors $|\mathbf{k}+\mathbf{G}|^2 \leq 30$ Ry and the Brillouin zone integrals are performed using a single $\mathbf{k}$-point at the corner $(\frac{1}{2}, \frac{1}{2}, \frac{1}{2})$ of the zone. Convergence tests show that the relative errors in total energies are ± 0.01 eV and in atomic positions are ± 0.02 Å. Vacancy or interstitial defects are simulated by re-

moving a Li ion from or by adding a Li ion to the supercell. The supercells have 127 atoms with 1 excess electron or 129 atoms with 1 deficient electron for the vacancy or interstitial simulations, respectively. The charged supercells are compensated with uniform background charge for the purpose of calculating the Coulomb interaction.

Experimental measurements have shown that the Li ion conductivity of polycrystalline[3] and single crystal[23] samples follows an Arrhenius temperature (T) dependence of the form

$$\sigma(T) = \frac{\sigma_0}{T} \mathrm{e}^{-E_A/k_B T}, \tag{1}$$

where σ_0 is a constant prefactor which depends on details of the sample and E_A is the activation energy. For extrinsic defects, E_A is the same as the migration energy of the defects, E_m. However, for intrinsic defects, using quasi-equilibrium statistical mechanics arguments,[24–26] it follows that $E_A = E_m + E_f/2$, where E_f is the formation energy of the vacancy-interstitial pair. In this work, estimates for the migration energies E_m for Li ion diffusion are calculated using the "nudged elastic band"[27–29] method (NEB) as implemented in the *PWscf* code. The basic assumptions of this approach[27] are that the diffusion is slow enough so that the processes are well described by Boltzmann statistics and so that the diffusion rate is controlled by processes which pass through harmonic regions of the potential energy surface near minima and saddle points which represent transition states of the system. The migration energies E_m are estimated from the energy difference of the lowest potential minimum and highest potential energy saddle point along the diffusion path. The computational effort is thus focused on finding the saddle points of the potential energy surfaces between local minimum energy configurations. For each of the diffusion paths considered, we find a series of steps characterized by pairs of local minimum energy configurations. The search for the saddle point is implemented by assuming 4-7 intermediate "images" between each pair of local minima. Each of the images is relaxed until the forces

perpendicular to the minimum energy path are less than 0.05 eV/Å. The energies between each pair of local minima are determined by interpolating between the energies of the images. We estimate that the accuracy of this interpolation allows us to estimate the migration energy between each pair of local minima within an error of ±0.05 eV. At each image, in addition to the energy, we can calculate a "configuration coordinate" which is a measure of the ion displacements at each image (I), scaled to the displacements of ions between the initial (i) and final (f) meta-stable configurations:

$$x_{iI} = \Delta X_{if} \frac{u_{iI}}{u_{if}} \quad \text{where} \quad u_{iI} \equiv \sum_{J=i+1}^{I} d_{JJ-1} \quad \text{and} \quad d_{JJ-1} \equiv \left| \sum_{a} (\mathbf{R}_J^a - \mathbf{R}_{J-1}^a) \right|. \qquad (2)$$

Here $\mathbf{R}_J^a$ denotes the atomic position of the a^{th} atom of the supercell for the J^{th} image. With this definition, for a supercell containing N atoms, d_{JJ-1} measures the $3N$-dimensional displacement between images and the configuration coordinate x_{iI} indicates the accumulated atomic displacement between the initial (i) and I^{th} meta-stable configurations, scaled by the physical displacement ΔX_{if} of the defect during this step.

III. CALCULATION RESULTS

A. Diffusion via vacancy mechanisms

As shown in Fig. 1, if a single Li ion is removed from the crystal, there are several neighboring Li ions which can hop into the vacancy site and contribute to a 3-dimensional diffusion. We have considered several possible diffusion paths along the 3 orthogonal lattice directions. Since there are two crystallographically inequivalent Li sites in this structure, there exist two metastable vacancy sites. We find that the total energies of vacancies at the

two inequivalent sites differ according to

$$E(\mathrm{Li}_{V(d)}) - E(\mathrm{Li}_{V(c)}) = 0.22 \text{ eV}, \tag{3}$$

using the crystallographic notation[11] for the d-type site of multiplicity 8 and the c-type site of multiplicity 4. Diffusion steps which involve these two different sites will therefore differ by ± 0.22 eV depending on whether the hopping direction is c-type $\rightarrow$ d-type or d-type $\rightarrow$ c-type.

We have identified 4 likely diffusion paths which are summarized in Table II, using the labels of Fig. 1 to indicate the vacancy positions. For each step in the path, we list the distance as measured from the corresponding perfect crystal sites and the maximal migration energy calculated from the NEB formalism for that step. The calculated migration barriers of Li vacancies show a slight anisotropy (0.6-0.7 eV) along the 3 crystallographic directions in γ-Li_3PO_4.

As evident from Fig. 1, vacancy diffusion generally involves zig-zag motions such as the $1(d) \leftrightarrow 2(c) \leftrightarrow 3(d)$ path for diffusion along the **a**-axis. Figure 2 summarizes the NEB results for this case, showing a smaller energy barrier for the first step and a 0.69 eV barrier for the overall process. For the **b**-axis, diffusion can proceed directly along the axis with hops between adjacent minimum energy sites of type d. The crystal structure is such that the distance between the $1 \leftrightarrow 4$ sites are slightly smaller than the distance between the $4 \leftrightarrow 5$ sites and the migration barrier is slightly smaller for the shorter path as shown in Fig. 3, with a 0.67 eV barrier for the overall process. One might expect to find a low migration barrier for the **b**-axis diffusion, since recent simulations[30, 31] for olivine $LiFePO_4$ have found Li ion diffusion to occur mainly along the 1-dimensional channels of its **b**-axis which appears to have some structural similarities to the **b**-axis Li ion channels in γ-Li_3PO_4. However, as shown in Table II and in Fig. 3, the migration energies for this path are comparable to those

of the **a**-axis. For vacancy diffusion along the **c**-axis, there are two possible zig-zag paths shown in Table II and in Fig. 4. The lowest migration energy that we have found occurs for the $4(d) \leftrightarrow 8(d) \leftrightarrow 7(d)$ path which consists of two equivalent segments with a net barrier of 0.56 eV.

B. Diffusion via interstitial mechanisms

While Li_3PO_4 has a reasonably closed packed structure, there exist other materials, such as the electrolyte Li_4SiO_4[32] and metallic Li in its bcc structure which have a higher density of Li ions; thus it is reasonable to expect the possibility of inserting interstitial Li ions into Li_3PO_4. In fact, viewing the crystal structure of γ-Li_3PO_4 along the **c** or **b** axes, reveals two types of the void channels. It is convenient to enumerate the meta-stable interstitial sites based on two geometrically distinct void channels along the **c**-axis, which we label "I" and "II". Figure 5 shows the equilibrium positions of the lowest energy configurations of an interstitial Li ion in each of those two channels, labeled I_0 and II_0, respectively, while Table III lists their relative energies and approximate positions in terms of fractional coordinates of the perfect crystal unit cell. Because of the Pnma crystal symmetry, within a unit cell there are 4 sites equivalent to the I_0 site and 8 sites equivalent to the II_0 site shown in Fig. 5 and in Table III. Figure 6 shows the relaxed structures of these same interstitial configurations viewed along the **b**-axis. In this view, it is apparent that configuration II_0 results in much more drastic lattice distortion particularly of nearest-neighbor c-type Li ions than does the I_0 configuration. In fact, as listed in Table III, there are two symmetry related meta-stable interstitial sites in channel II equivalent to the II_0 site separated by saddle point which we label II^* at the center of the cell. Note that II^* is located at a-site in the crystal with Pnma symmetry so that there are 4 equivalent sites per unit cell. An

NEB simulation using an initial path which includes an image slightly perturbed from the high symmetry II^* configuration confirms that it is a saddle point and not a higher order maximum of the potential energy surface. In Table III we also list a higher energy meta-stable interstitial configuration found in channel I. While undoubtedly there are additional meta-stable interstitial sites, the structures listed in Table III represent the relaxed structures obtained from a general scan of reasonable trial geometries.

Each diffusion step of the interstitial Li ion involves two of the meta-stable configurations listed in Table III or their equivalence, showing the interstitial diffusion is the most efficient ion transport. We have found that diffusion between I_0 (−0.30, 0.75, 1.00) and its equivalent I_0 (−0.20, 0.25, 0.50) sites takes place most efficiently via concerted motion of the interstitial Li ion and a neighboring Li ion at a d-type site of the host lattice which is referenced in the literature[24, 25, 33] as an interstitialcy mechanism. During the interstitialcy process, an interstitial Li ion at an I_0 site kicks out and replaces a neighboring d-type Li of the host lattice while the "kicked-out" Li ion takes an equivalent interstitial I_0 site. As shown in Fig. 7, the NEB results indicate that the migration energy for this interstitialcy step is $E_m = 0.21$ eV. Diffusion along the **b** and **c** axes for an interstitial ion in any "I" type channel can thus be described as a series of zig-zag steps with this mechanism. This interstitialcy process is by far more efficient energetically than any of the other interstitial diffusion mechanisms we have considered including direct hopping between I_0 and neighboring I_0 or I_1 sites.

Diffusion along the **a**-axis involves processes in both the I and II type void channels. One possible mechanism is summarized in Table IV and in Fig. 8, involving an interstitial ion at an I_0 site at (0.30, 0.25, 1.00) diffusing to an equivalent I_0 site at (0.70, −0.25, 0.00) with an overall migration energy of $E_m = E(II^*) - E(I_0) = 0.35$ eV. This diffusion consists of three steps: (1) $I_0 \leftrightarrow II_0$, (2) $II_0 \leftrightarrow II^* \leftrightarrow II_0$, and (3) $II_0 \leftrightarrow I_0$. For the diffusion step

1 which has an energy barrier of 0.23 eV[34], an interstitial Li ion at an I_0 site (0.30, 0.25, 1.00) kicks a neighboring c-type Li ion of the host lattice into a II_0 configuration with the interstitial site (0.52, 0.07, 0.57). For the diffusion step 2 within the type II void channel, the Li ion at the interstitial II_0 site performs a direct hop to its equivalent II_0 site (0.48, -0.07, 0.43) via the saddle point configuration II^* (0.50, 0.00, 0.50), resulting in a 0.17 eV barrier. For the diffusion step 3, the Li ion at the interstitial II_0 site kicks out another distorted c-type Li ion of the host lattice into an I_0 configuration (0.70, -0.25, 0.00). It is worth noting that this mechanism has an inversion symmetry centered at the saddle point configuration II^* at the site (0.50, 0.00, 0.50).

The simulations of the interstitialcy mechanism described here for diffusion within the type-I void channels or for diffusion between type-I and type-II void channels suggest possible mechanisms for interstitial Li ion diffusion in all 3 crystallographic directions. The calculated migration energies of $E_m = 0.35$ eV for the **a**-axis diffusion and $E_m = 0.21$ eV for the **b**- or **c**-axis diffusion are considerably smaller than experiment[3, 23, 32, 35] and smaller than the calculated barriers for the vacancy mechanisms.

C. Formation energies for vacancy-interstitial pairs of defects

By definition, in a perfect crystal no vacancies or interstitial ions can exist, so that mobile species such as vacancies and interstitials must first be created before ion diffusion can occur. In real crystals, intrinsic defects (vacancy-interstitial pairs) are created thermally with a formation energy E_f. Hence the resulting conductivity has an activation energy of $E_A = E_m + E_f/2$. We have estimated the formation energy for a Li ion vacancy-interstitial pair using our supercells. So far, the lowest energy for the defect formation is found to be $E_f \approx 1.6$ eV in γ-Li_3PO_4, formed by relaxing the initial geometry of an interstitial ion in

an I_0 site and a next neighbor vacancy in a c-site. (Using the nearest neighbor vacancy site, the system relaxes into the perfect crystal geometry.) The interstitial diffusion with a migration barriers of $E_m = 0.2 - 0.4$ eV dominate the vacancy diffusion with a migration barriers of $E_m = 0.6 - 0.7$ eV in the crystal. Using the migration barriers for interstitials, we can estimate activation energy, E_A, of ion diffusion within a crystalline γ-Li_3PO_4 and compare it to the measurements on aligned single crystals[23] in Table V. The computed activation barriers of $E_A = 1.0 - 1.2$ eV agree well with the experimental results of 1.1-1.2 eV, varying slightly along the three crystallographic directions. In addition, our results show the interstitial diffusion along the **b** and **c** axes to have the same atomistic mechanism (see Fig. 7), which is consistent with the fact that the activation barriers along the **b** and **c** axes are measured to be the same in the experiment.[23] Other authors[3, 32, 35] have reported activation energies of 1.2-1.3 eV for polycrystalline samples of γ-Li_3PO_4 which are also in good agreement with our calculated results.

IV. CONCLUSIONS

In summary, we have identified the vacancy and interstitial diffusion mechanisms of Li ions in all 3 crystallographic directions of γ-Li_3PO_4. The vacancy diffusion is slightly anisotropic, with the lowest migration energy occurring for zig-zag paths along the **c**-axis determined to be $E_m = 0.56$ eV. The interstitial diffusion is also slightly anisotropic and involves interstitialcy mechanisms which result in a much lower migration energies of $E_m = 0.21$ eV for diffusion along the **b** and **c** axes and $E_m = 0.35$ eV for diffusion along the **a**-axis. Since it has lower migration barriers, the interstitial diffusion mechanism dominates the vacancy diffusion mechanism, provided that interstitial defects are present or can be created. Intrinsic defects control the diffusion process in single crystals[23] and polycrystalline samples,[3, 32, 35]

where the activation energies are found to be $E_A = 1.1 - 1.3$ eV. The formation energy of intrinsic defects (a vacancy-interstitial pair) is computed to be $E_f = 1.6$ eV. The resulting activation energies of intrinsic defects are $E_A = 1.0 - 1.2$ eV along the 3 crystallographic directions, in good agreement with the experiments. The diffusion along the **b** and **c** axes are found to be controlled by the same atomistic mechanism, consistent with the experimental results[23] which find E_A to be the same for these two crystal orientations.

In crystals prepared with a measurable number of extrinsic vacancies, the measured activation energy is considerably reduced. For example, Wang and co-workers [3] prepared a crystal with the measured stoichiometry of $Li_{2.88}PO_{3.73}N_{0.14}$, which has 12% Li vacancy per formula unit approximately adjusted for charge neutrality. For this material, the activation energy was measured to be $E_A = 0.97$ eV, reduced by 0.27 eV from that of the pure material. The Oak Ridge group also has measured the activation energies of thin films of this material with varying Li content (as well as the introduction of varying amounts of N), finding activation energies between $E_A \approx 0.6 - 0.7$ eV. Considerably more calculations will be needed to determine whether the mechanisms we have modeled for the crystalline material have any validity for the thin films. However, it is reassuring to note that materials with non-stoichiometric amounts of Li show activation energies comparable to E_m values calculated for the vacancy diffusion mechanism.

On the basis of our modeling, we believe that the interstitialcy mechanism should provide the most efficient ion transport. Perhaps the fact that this has not yet been verified by experiment can be attributed to the fact that samples with excess Li ions have not been prepared. Nevertheless, an early study of Li_4SiO_4-Li_3PO_4 solid solutions[32] has shown that a Li_4SiO_4-Li_3PO_4 solid solution with a 0.6 mole fraction of Li_3PO_4 has the lowest activation energy of $E_A = 0.5$ eV compared to the $E_A = 1.3$ eV activation energy for pure Li_3PO_4. It

is expected that the Li_4SiO_4-Li_3PO_4 solid solution may contain a significant concentration of Li interstitials, which could perhaps contribute to the reduction in activation energy. The computed migration energy of $E_m = E_A = 0.2 - 0.4$ eV for Li ion interstitials is lower than the measured $E_A = 0.5$ eV activation energy in the Li_4SiO_4-Li_3PO_4 solid solution. It would be interesting to perform additional calculations to see if this might be due to the structural difference between the Li_4SiO_4-Li_3PO_4 solid solutions and the pure γ-Li_3PO_4 or perhaps due to trapping defects.

The results reported here have identified the main basic processes involved with Li ion diffusion in Li_3PO_4 materials. In future work, [36] we will investigate the effects of the crystalline structure by comparing results for the γ structure with those for the β structure, as well as comparing the effects of the form of the exchange-correlation functional. In addition, we will consider the effects of N doping and O vacancies. Cluster calculations reported in the literature[37] find N to have a significant effect on the migration barrier of Li ion vacancies. The actual barriers reported in that work are considerably larger than those reported here. In addition, we plan to consider interface effects which might also provide sources and sinks for defects. In electrolyte applications, the interface can have significant effects on the Li ion transport, compared with the bulk effects discussed here.

Acknowledgments

This work was supported by NSF grants NSF DMR-0405456 and DMR-0427055, and benefited from discussions with R. E. Noftle, G. E. Matthews, W. C. Kerr, Ping Tang, and Xiao Xu at Wake Forest University, Richard Hennig at Cornell University, and Dallas Trinkle at the University of Illinois, as well as from helpful advice from Dr. Nancy J. Dudney of Oak Ridge National Laboratory. Computational results were obtained using the DEAC

cluster, and benefited from storage hardware awarded to Wake Forest University through an IBM SUR grant.

[1] J. B. Bates, N. J. Dudney, G. R. Gruzalski, R. A. Zuhr, A. Choudhury, D. F. Luck, and J. D. Robertson, Solid State Ionics **53–56**, 647 (1992).

[2] J. B. Bates, N. J. Dudney, G. R. Gruzalski, R. A. Zuhr, A. Choudhury, D. F. Luck, and J. D. Robertson, Journal of Power Sources **43–44**, 103 (1993).

[3] B. Wang, B. C. Chakoumakos, B. C. Sales, B. S. Kwak, and J. B. Bates, Journal of Solid State Chemistry **115**, 313 (1995).

[4] X. Yu, J. B. Bates, J. G. E. Jellison, and F. X. Hart, Journal of the Electrochemical Society **144**, 524 (1997).

[5] N. J. Dudney, in *Lithium Batteries: Science and Technology*, edited by G.-A. Nazri and G. Pistoia (Klumwer Academic Publishers, 2004), chap. 20, pp. 623–642, iSBN 1-4020-7628-2.

[6] J. Zemann, Acta Cryst. **13**, 863 (1960).

[7] C. Keffer, A. Mighell, F. Mauer, H. Swanson, and S. Block, Inorganic Chemistry **6**, 119 (1967).

[8] O. V. Yakubovich and V. S. Urusov, Crystallography Reports **42**, 261 (1997).

[9] L. Popović, B. Manoun, D. de Wall, M. K. Nieuwoudt, and J. D. Comins, Journal of Raman Spectroscopy **34**, 77 (2003).

[10] R. M. Rojas, J. L. M. de Vidales, A. Delgado, and J. V. Sinisterra, Journal of Solid State Chemistry **106**, 237 (1993).

[11] T. Hahn, ed., *International Tables for Crystallography, Volume A: Space-group symmetry, Fifth revised edition* (Kluwer, 2002), ISBN 0-7923-6590-9.

[12] P. Hohenberg and W. Kohn, Physical Review **136**, B864 (1964).

[13] W. Kohn and L. J. Sham, Physical Review **140**, A1133 (1965).

[14] S. Baroni, A. D. Corso, S. de Gironcoli, P. Giannozzi, C. Cavazzoni, G. Ballabio, S. Scandolo, G. Chiarotti, P. Focher, A. Pasquarello, et al., available from the website http://www.pwscf.org/.

[15] D. Vanderbilt, Phys. Rev. B **41**, 7892 (1990), USPP code is available from the website http://www.physics.rutgers.edu/ dhv/uspp/.

[16] P. Tang, Ph.D. thesis, Wake Forest University (2006).

[17] P. Tang, N. A. W. Holzwarth, and Y. Du, manuscript in preparation.

[18] J. P. Perdew and Y. Wang, Phys. Rev. B **45**, 13244 (1992).

[19] J. P. Perdew, K. Burke, and M. Ernzerhof, Phys. Rev. Lett. **77**, 3865 (1996), erratum – Phys. Rev. Let. **78**, 1396 (1997).

[20] A. Kokalj, Journal of Molecular Graphics and Modeling **17**, 176 (1999).

[21] OpenDX – The Open Source Software Project Based on IBM's Visualization Data Explorer – is available from the web site http://www.opendx.org.

[22] M. Parrinello and A. Rahman, J. Appl. Phys. **52**, 7182 (1981).

[23] A. K. Ivanov-Shitz, V. V. Kireev, O. K. Mel'nikov, and L. N. Demainets, Crystallography Reports **46**, 864 (2001).

[24] A. R. West, *Basic Solid State Chemistry, Second Edition* (John Wiley & Sons, Inc., 2000), ISBN 0-471-98756-5.

[25] D. M. Smith, *The Defect Chemistry of Metal Oxides* (Oxford University Press, 2000), ISBN 0-19-511014-5.

[26] The argument can be summarized by assuming that ionic conductivity is related to the temperature T, migration energy E_m, and concentration of mobile ions n according to $\sigma \cdot T \propto n\mathrm{e}^{-E_m/k_BT}$. For extrinsic defects, the concentration of mobile ions n is determined by

the doping process and is independent of temperature. For intrinsic defects, the concentration of mobile ions n is determined by the formation of vacancy-interstitial pairs. We can assume that these defects are formed by a perfect crystal ion moving into an interstitial site, ensuring an equal number of vacancies and interstitials with a formation energy E_f. Under conditions of thermal equilibrium, the concentration (n) of vacancies and interstitials is determined by a Boltzmann factor $n^2 \propto \mathrm{e}^{-E_f/k_BT}$ and $n \propto \mathrm{e}^{-E_f/2k_BT}$.

[27] G. Henkelman, B. P. Uberuaga, and H. Jónsson, J. Chem. Phys. **113**, 9901 (2000).

[28] G. Henkelman and H. Jónsson, J. Chem. Phys. **113**, 9978 (2000).

[29] H. Jónsson, G. Mills, and K. W. Jacobsen, in *Classical and Quantum Dynamics in Condensed Phase Simulations*, edited by B. J. Berne, G. Ciccotti, and D. F. Coker (World Scientific, Singapore, 1998), p. 385.

[30] D. Morgan, A. V. der Ven, and G. Ceder, Electrochemical and Solid-State Letters **7**, A30 (2004).

[31] C. Ouyang, S. Shi, Z. Wang, X. Huang, and L. Chen, Phys. Rev. B **69**, 104303 (2004).

[32] Y.-W. Hu, I. D. Raistrick, and R. A. Huggins, Journal of the Electrochemical Society **124**, 1240 (1977).

[33] W. Hayes and A. M. Stoneham, *Defects and Defect Processes in Nonmetallic Solids* (John Wiley & Sons, Inc., 1985), ISBN 0-471-89791-4.

[34] The dip in the energy path between I_0 and II_0 (Fig. 8) is very sensitive to the details of the NEB calculation. If fewer images are used, the small dip can be missed and E_m can be overestimated by 0.03 eV which is consistent with the $\pm$0.05 eV general error estimate for the NEB calculations in this work.

[35] R. A. Huggins, Electrochimica Acta **22**, 773 (1977).

[36] Y. A. Du, N. A. W. Holzwarth, and X. Xu, manuscript in preparation.

[37] H. Rabaâ, R. Hoffmann, N. C. Hernández, and J. F. Sanz, Journal of Solid State Chemistry **161**, 73 (2001).

TABLE I: Lattice constants and fractional atomic coordinates of inequivalent atomic positions for γ-Li_3PO_4.

		Ref. [6]	Ref. [3]	Ref. [8]	This work.
a (Å)		10.53	10.4612	10.490	10.58
b (Å)		6.12	6.1113	6.120	6.17
c (Å)		4.93	4.9208	4.9266	4.99
Li(d)	x	0.162	0.1627	0.1639	0.164
	y	0.495	0.5016	0.5013	0.502
	z	0.304	0.3008	0.3013	0.303
Li(c)	x	0.422	0.4246	0.4237	0.425
	y	0.75	0.75	0.75	0.75
	z	0.196	0.2045	0.2056	0.202
P(c)	x	0.411	0.4115	0.41151	0.412
	y	0.25	0.25	0.25	0.25
	z	0.308	0.3079	0.30878	0.308
O(d)	x	0.342	0.3418	0.34167	0.341
	y	0.042	0.0441	0.04289	0.043
	z	0.205	0.2054	0.2057	0.205
O(c)	x	0.052	0.0503	0.05042	0.051
	y	0.25	0.25	0.25	0.25
	z	0.295	0.2928	0.2937	0.297
O(c)	x	0.090	0.0896	0.08964	0.089
	y	0.75	0.75	0.75	0.75
	z	0.125	0.1223	0.1223	0.122

TABLE II: Vacancy diffusion steps

Net direction	Step[a]	Net distance[b]	E_m[c]
a	$1(d) \leftrightarrow 2(c)$	2.95	0.36
	$2(c) \leftrightarrow 3(d)$	3.20	0.69
	$1(d) \leftrightarrow 2(c) \leftrightarrow 3(d)$	5.31	0.69
b	$1(d) \leftrightarrow 4(d)$	3.06	0.45
	$4(d) \leftrightarrow 5(d)$	3.11	0.67
	$1(d) \leftrightarrow 4(d) \leftrightarrow 5(d)$	6.17	0.67
c	$4(d) \leftrightarrow 8(d)$	3.09	0.56
	$4(d) \leftrightarrow 8(d) \leftrightarrow 7(d)$	4.99	0.56
	$4(d) \leftrightarrow 6(c)$	3.51	0.55
	$6(c) \leftrightarrow 7(d)$	2.70	0.63
	$4(d) \leftrightarrow 6(c) \leftrightarrow 7(d)$	4.99	0.63

[a]Labels defined in Fig. 1.

[b]Equivalent perfect crystal distances in Å measured before relaxation.

[c]Maximum energy barrier in eV between these two sites, hopping in either direction.

TABLE III: Parameters of some meta-stable interstitial sites.

Label	Energy[a]	x[b]	y	z
I_0	0.00	0.30	0.25	0.00
I_1	0.78	0.28	0.25	0.59
II_0	0.18	0.52	0.07	0.57
II^*	0.35	0.50	0.00	0.50

[a]Energies are given relative to the energy of the I_0 configuration in units of eV.

[b]Coordinates of the interstitial site are given as fractional coordinates of the perfect crystal structure listed in Table I.

TABLE IV: Interstitial diffusion steps

Type	Step	Net distance[a]	E_m[b]
interstitialcy	$I_0 \leftrightarrow I_0$	4.1	0.21
interstitialcy	$I_0 \leftrightarrow II_0$	3.4	0.23
direct hop	$II_0 \leftrightarrow II^*$	0.6	0.17
	$I_0 \leftrightarrow II_0 \leftrightarrow II^* \leftrightarrow II_0 \leftrightarrow I_0$	7.2	0.35

[a]Equivalent perfect crystal distances in Å measured before relaxation.

[b]Maximum energy barrier in eV between these two configurations.

TABLE V: Activation energies E_A (eV) for Li ion conductivity in crystalline γ-Li_3PO_4.

Net direction	E_A (this work)	E_A (exp.[a])
a	1.2	1.23
b	1.0	1.14
c	1.0	1.14

[a]Ref. [23]

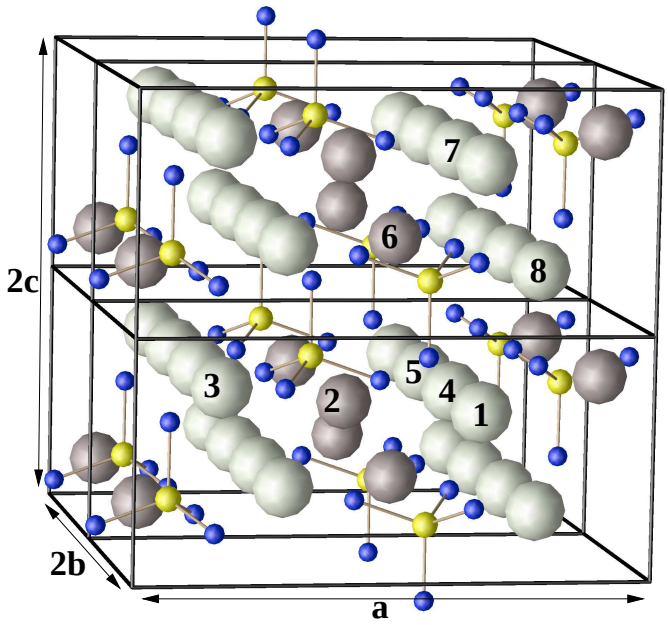

FIG. 1: (Color online) Ball and stick drawing of the Pnma crystal structure of γ-Li_3PO_4. Li ions are indicated by light and dark gray balls representing the inequivalent $d(8)$ and $c(4)$ sites[11], respectively. The P and O ions are indicated by small balls and sticks (colored on line yellow and blue respectively). The four unit cells shown in the drawing represent the supercell used in the present work. The labels indicate possible Li vacancy sites explained in the text.

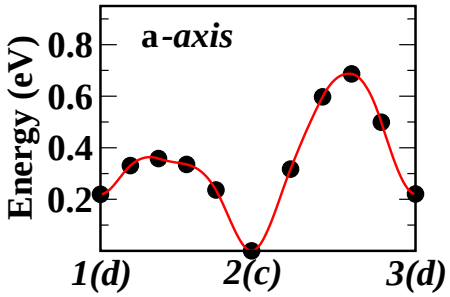

FIG. 2: (Color online) Diagram of **a**-axis energy path for vacancy diffusion plotted along the configuration coordinate (Eq. 2). The zero of energy is taken as the energy of a Li-ion vacancy in a *c*-type site as calculated from our supercell.

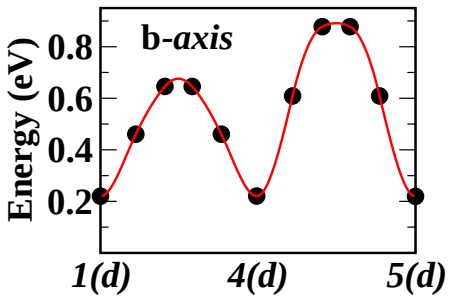

FIG. 3: (Color online) Diagram of **b**-axis energy path for vacancy diffusion similar to Fig. (2).

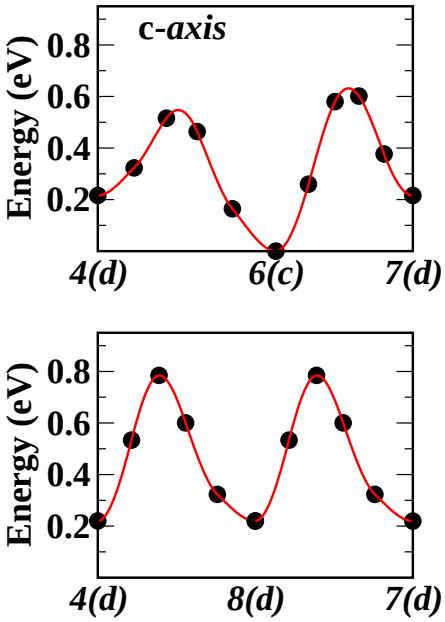

FIG. 4: (Color online) Diagram of **c**-axis energy path for vacancy diffusion similar to Fig. (2), showing two possible diffusion paths.

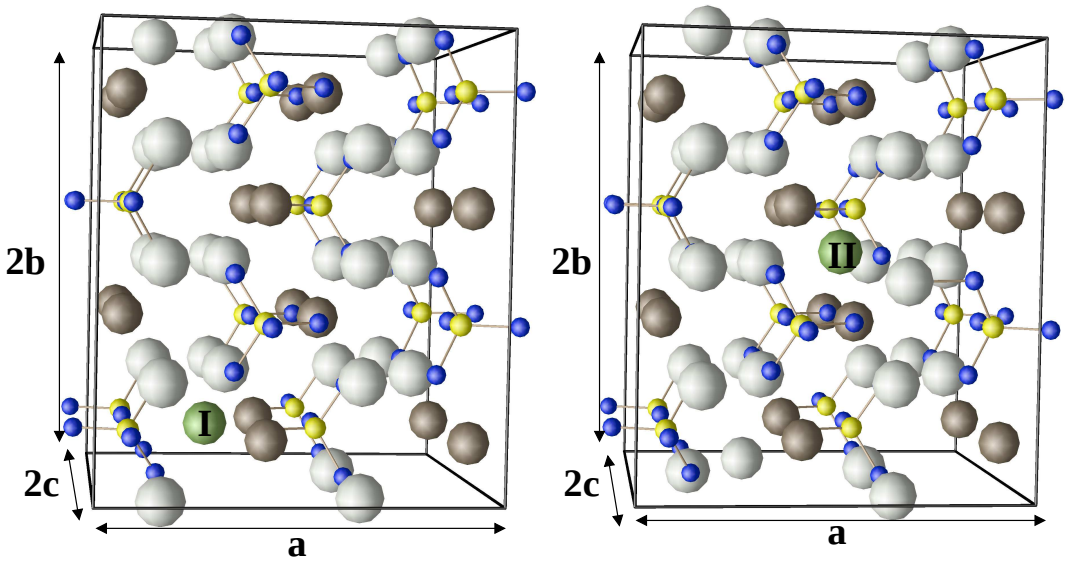

FIG. 5: (Color online) Ball and stick drawing of meta-stable interstitial Li ion configurations viewed along the **c**-axis using the same conventions as Fig. 1 with the interstitial sites labeled I (left) and II (right) (colored green on line). These correspond to the I_0 and II_0 sites respectively, as listed in Table III.

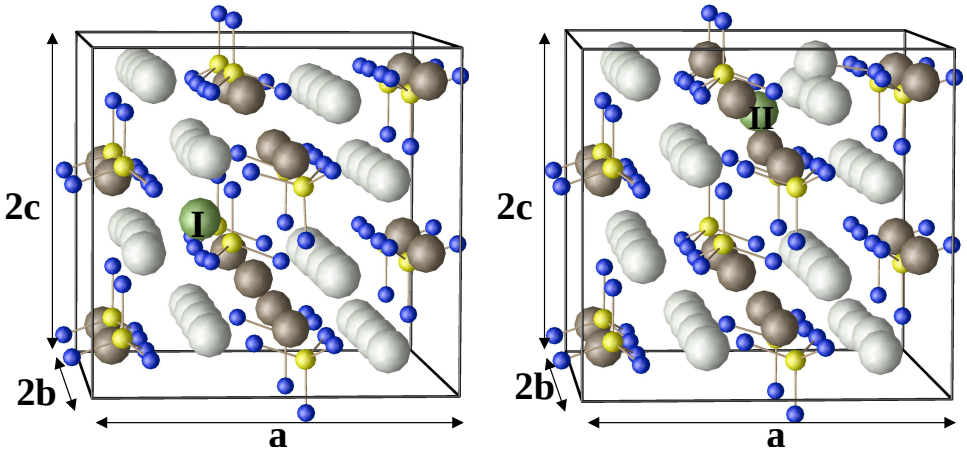

FIG. 6: (Color online) Interstitial configurations shown in Fig. 5 viewed along the **b**-axis.

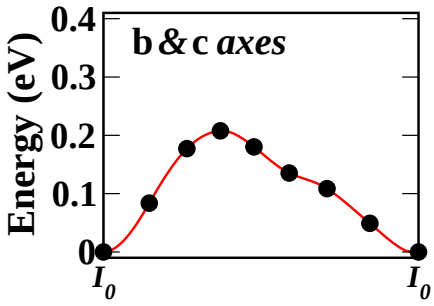

FIG. 7: (Color online) Diagram of energy path for interstitial diffusion along the **b** and **c** axes between adjacent I_0 configurations via an interstitialcy mechanism.

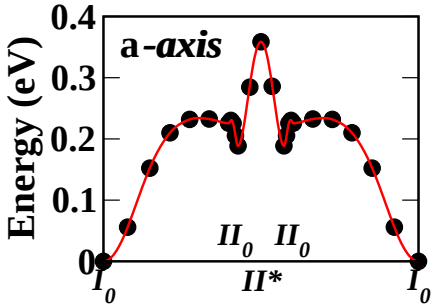

FIG. 8: (Color online) Diagram of energy path for interstitial diffusion along the **a** axis between adjacent I and II channel sites using a combination of interstitialcy and direct hop steps.